Available online at www.sciencedirect.com
ScienceDirect
Ceramics International 35 (2009) 2933–2942
CERAMICS INTERNATIONAL
www.elsevier.com/locate/ceramint

Fabrication, characterization and bioactivity evaluation of calcium pyrophosphate/polymeric biocomposites

Abeer M. El Kady *, Khaled R. Mohamed, Gehan T. El-Bassyouni

National Research Centre, Biomaterials Department, Behoos Street, Dokki, Giza, Egypt

Received 24 June 2008; received in revised form 10 February 2009; accepted 30 March 2009
Available online 24 April 2009

Abstract

The design of the biocomposites offers the opportunity to create grafting materials with excellent bioactivity, resorbability and improved mechanical properties. In this study, we are concerned with the preparation of calcium pyrophosphate (CPP) and its composites with polymeric matrix to enhance these properties. The fabricated biocomposites were characterized by X-ray diffraction (XRD), Fourier transformer infrared spectra (FT-IR), thermogravimetric (TGA) analyses and scanning electron microscope with X-ray elemental analysis (SEM-EDAX). The characterization results confirmed homogeneity, interaction and integration between the CPP filler and polymeric matrix. The mechanical properties of biocomposites had enhanced values compared to the original copolymer matrices and were comparable to those of cancellous bone. *In vitro* test results via calcium and phosphorous ions measurements, showed that the biocomposites had enhanced ability to accelerate the mineralization of calcium phosphate layer on their surfaces. FT-IR and SEM-EDAX post-immersion confirmed that the CPP/polymeric composites containing chitosan or chitosan–gelatin matrix had ability to induce a bone-like apatite layer onto their surfaces. Finally, a novel CPP/polymeric biocomposites have good bioactivity and suitable mechanical properties; therefore, they could be used in bone grafting and tissue engineering applications in future.

Keywords: Calcium pyrophosphate; Biocomposites; *In vitro*; SEM-EDAX

1. Introduction

Recently a great deal of interest has been directed towards creating bioactive ceramic/polymer composites to be used as a bone grafting materials and in tissue engineering applications. Bone grafts have been used to fill bone defects caused by disease or trauma, such as bone fractures, infections, and tumors [1]. Over the past decade, the main goal of bone tissue engineering has been to develop biodegradable materials as bone graft substitutes for filling large bone defects [2]. These materials should maintain adequate mechanical strength, be osteoconductive, and degrade at a controlled rate to provide space for the formation of new bone. A biodegradable material is attractive because it may be eventually replaced by host tissue while at the same time providing the initial structural strength and integrity necessary for regeneration of critical size bone defects. Because no single existing material possesses all the necessary properties required in an ideal bone graft, there is a growing interest in composite materials [3].

Therefore, the development of biocomposites with good mechanical properties, excellent bioactivity and biocompatibility similar to natural bone to meet the need of hard tissue repair has been a hot topic for over 30 years [4]. To obtain an advanced mechanical performance of the bioactive composite, bioceramic particles were usually incorporated into the polymer matrix [5]. There has been widespread use of calcium phosphate bioceramics for bone regeneration applications. However, their clinical applications have been limited because of their brittleness and difficulty of shaping [6]. Calcium phosphate ceramic has poor mechanical properties and the use of biodegradable polymer/bioceramic composites could be a solution to this problem. The addition of biodegradable polymers to calcium phosphate ceramics would allow for better manipulation and control over both the macro- and micro-structure in shaping composites to fit bone defects. In addition, biodegradable polymers can be used as binders for ceramic to reduce their brittleness [7]. Moreover, the addition of ceramic granules can serve to reinforce and stiffen the polymeric matrix [8].

* Corresponding author. Fax: +202 333 70931.
E-mail address: abeerelkady_2000@yahoo.co.uk (A.M. El Kady).

0272-8842/$36.00
doi:10.1016/j.ceramint.2009.03.042

Bioresorbable synthetic polymers have attracted increasing attention for their use as tissue engineering scaffolds and as a bone grafting materials in the last 10 years [9]. However, a number of problems have encountered regarding the use of biodegradable polymers in these applications. One of the limitations of these polymers is the lack of bioactivity so that the new bone tissue cannot bond to the polymer surface tightly. Another problem is that they may not completely meet the requirements for some applications due to their insufficient mechanical properties. Amongst the approaches that have been followed to overcome these limitations, in the first approach, different polymers and monomers have been combined together as copolymers in order to obtain a wide range of properties. In the second approach, the incorporation of calcium phosphate ceramics and glasses into the polymeric matrix would improve not only the mechanical properties of the material, but also its bioactivity and biological behavior [10]. The design of polymer/ceramic composites offers the opportunity to create a grafting material with tailored bioactivity, resorbability and improved mechanical properties. The resorbability of the designed material can be engineered to match the rate of new bone formation.

Recently much attention has been given to utilize chitosan in biomedical applications such as space filling implants [11]. Chitosan is biodegradable, biocompatible and non-toxic [12]. The surface of chitosan is hydrophilic, which facilitates cell adhesion, proliferation, and differentiation [13]. Despite its otherwise attractive properties, porous chitosan scaffolds are lack of mechanical strength and may not be suitable for tissue engineering of hard tissue [14]. In addition, chitosan is not bioactive, only biotolerant and will be surrounded by fibrous tissue when embedded in the body. The incorporation of calcium phosphate ceramic into chitosan matrix has been shown to increase osteoconductivity and biodegradability [15], with significant enhancement of mechanical strength [16].

Gelatin is a soluble protein derived from partially denatured collagen. Attractive properties of gelatin, such as good biocompatibility, low immunogenicity, promotion of cell adhesion and growth, and low cost, make it ideally suitable as a biomaterial for tissue engineering [17]. Gelatin contains free carboxyl groups on its backbone and has the potential to blend with chitosan to form a network by hydrogen bonding [18]. The incorporation of calcium phosphate ceramic into chitosan–gelatin composite has been recently shown to increase its osteoconductivity as well as improving stem cells adhesion and differentiation [19]. Recently, the use of 2-hydroxyethyl methacrylate (HEMA)-based polymer as a biocompatible material has been well-established. Poly(hydroxyethyl methacrylate) (poly(HEMA)) is well tolerated by biological tissues and has been used in a number of biomedical applications [15,20].

HA is known to exhibit limited osteoconduction and has a slow rate of degradation in physiological solutions because of its chemical stability [21]. On the other hand, several intermediate calcium phosphate phases can be discerned in the biomineralization process, which perhaps are also attractive from an implantological point of view. Hence, the use has already been made of the minerals burshite ($CaHPO_4{\cdot}2H_2O$) and octacalcium phosphate (OCP: $Ca_4H(PO_4)_3{\cdot}2.5H_2O$) [22]. These materials show the remarkable property that they are resorbed during time after implantation with a subsequent increase in bone tissue formation [23]. The mineral phase calcium pyrophosphate (CPP: $Ca_2P_2O_7$) is one of the intermediate products in biomineralization process. In bone, CPP can regulate the onset of calcification and can act as a trigger mechanism to promote mineralization. It can also alter the rate of crystal growth and dissolution [24]. In view of this suggested benefit, several studies focus on the use of CPP as coating material for dental and orthopedic implants. In addition, the results of an *in vitro* osteoblasts cell culture and *in vivo* animal study demonstrated that pyrophosphate is biocompatible with bone cells and has a great potential as an *in vivo* biodegradable bone substitute [25].

1.1. Aim of the work

Preparation of CPP filler powder from burshite powder was performed. The loading of CPP powder onto the polymeric matrix during the copolymerization process containing chitosan and/or chitosan gelatin for improving the bioactivity, biodegradation as well as the mechanical properties was carried out. The characterization of the prepared biocomposites to verify the homogeneity between two matrices, and *in vitro* test was performed, to insure the formation of apatite layer onto the surface of the materials.

2. Materials and methods

2.1. Materials

Calcium hydrogen phosphate dihydrate (burshite) was purchased from (Fluka) Chitosan polymer ($C_6H_{11}NO_4$) (high molecular weight and Brookfield viscosity: 800,000 cps), 2-hydroxyethylmethacrylate monomer ($CH_2{=}CCH_3$ COO C_2H_4OH) was provided by (Aldrich). Gelatin powder (from bovine skin) was purchased from the Sigma Chemical Co. The chemical initiators, cerric ammonium nitrate (CAN) $(NH_4)_2[Ce(NO_3)_6]$ (BDH Chemical Ltd., Poole, UK), sodium hydrogen sulphite and ammonium per sulphate were used to graft HEMA monomer onto chitosan and gelatin polymers.

2.2. Methods

2.2.1. Preparation of calcium pyrophosphate (CPP)

CPP was prepared through the dehydration and decomposition of burshite by heating treatment. Briefly, burshite powder was compacted at 1200 MPa pressures into 15 mm diameter cylindrical samples which were fired at 800 °C with soaking time for 3 h to transform burshite into CPP compound. The firing temperature at 800 °C was used to convert completely burshite to CPP compound. The prepared samples were ground and sieved up to size <150 μm.

2.2.2. Preparation of grafted chitosan copolymer

Chitosan (0.15 g) was dissolved in 8 ml of 3% acetic acid, 2 ml of HEMA monomer was added to chitosan solution, well

mixed and then 0.15 g of CAN initiator was also added to graft HEMA monomer onto the chitosan polymer. The mixture was put in water bath at 40 °C for 3 h to achieve the copolymerization process. The copolymer mixture (1) was left overnight at ambient temperature and then washed with hot ethanol with stirring for 1 h to remove the homopolymer. The mixture was filtered then collected and dried at 60 °C for 24 h. The grafting (*G%*) is calculated according to the following equation [26]. The produced grafted chitosan copolymer is denoted as copolymer:

$$G\% = \frac{W - W_0}{W_0} \times 100$$

W is the weight of grafted chitosan and W_0 is the weight of original chitosan.

2.2.3. Preparation of (CPP)/chitosan polymeric composites

Fixed weight (1.5 g) from CPP powder was well dispersed and mixed with the copolymer mixture (1) from the above experiment after 2.5 h from the copolymerization process and kept at 40 °C in water bath for 30 min. The CPP/chitosan polymeric composite was left overnight at ambient temperature and then the mixture was washed with hot ethanol with stirring for 1 h to remove homopolymer. The mixture was filtered, collected and dried at 60 °C overnight. The grafting of copolymer in the presence of filler (CPP powder) was calculated according to the following equation:

$$G\% = \frac{W_1 - W_0}{W_0} \times 100$$

where W_1 is the weight of grafted chitosan in the presence of the filler and W_0 is the weight of original chitosan.

2.2.4. Preparation of CPP/chitosan–gelatin polymeric composites

Chitosan polymer (0.075 g) was dissolved in 4.0 ml of 3% acetic acid solution and 1 ml of HEMA monomer was added to chitosan solution, well mixed and then 0.075 g of CAN initiator was added to graft HEMA monomer onto chitosan polymer. The mixture was well mixed and kept in a water bath at 40 °C for 2 h to obtain a homogenous copolymer mixture which is denoted as solution (1). Meanwhile, gelatin (0.1 g) was dissolved in 4 ml distilled water, 1 ml of HEMA monomer was added to gelatin solution, well mixed and then a mix equal weight from initiators (0.05 sodium hydrogen sulphate + 0.05 ammonium per sulphate) was added to graft monomer onto gelatin polymer. The mixture was put in water bath at 40 °C for 2 h to obtain a homogenous copolymer mixture denoted as solution (2). The two homogenous copolymer solutions (1) and (2) were well mixed and incubated at 40 °C for 30 min in water bath. Fixed weight 1.5 g from CPP filler powder was dispersed in the copolymer mixture, then well mixed and incubated for 30 min under the above conditions to complete the grafting process in the presence of the filler. The loaded copolymer mixture was left overnight at room temperature, then washed, filtered and dried at 60 °C overnight. The grafting % in the presence of CPP filler was calculated according the following equation:

$$G\% = \frac{W_2 - W}{W} \times 100$$

where W_2 is the weight of grafted chitosan–gelatin in the presence of 1.5 g of CPP filler and W is the weight of chitosan and gelatin polymers.

2.3. Characterization

The phase purity of sintered powder was examined by X-ray diffractometer Diana Corporation (USA) equipped with Co Kα radiation, λ = 1.79026 Å with Fe filter. The thermo-gravimetric analysis of the prepared copolymer and composite samples was carried out using a Perkin-Elmer (USA) thermogravimetric analyzer in air. The measurements were performed in air with a heating rate of 10 °C/min within the temperature range of 50–1000 °C. The infrared spectra of the sintered powder was obtained in the range 4000–400 cm^{-1} using KBr technique by using Fourier transformer infrared spectrophotometer (FT-IR) NEXAS 670, Nicolet, USA. FT-IR analysis was also carried out for the samples pre- and post-immersion to confirm the formation of apatite layer onto the surface. The surface morphology and elemental composition of the prepared copolymer and composite samples was examined with a JXA 840A Electron Probe Micro Analyzer (JEOL, Japan). The scanning electron microscope measurement for each sample was carried out at different magnification. The surface of samples were also analyzed pre- and post-immersion 21 days in simulated body fluid (SBF) using scanning electron microscopy (SEM) coupled with energy dispersive X-ray analysis (SEM/EDAX) to determine the calcium/phosphorus ratio for surface apatite onto the copolymer and composite samples. For SEM, the substrates were mounted on metal stubs and coated with carbon before examination.

2.4. Mechanical testing

The composites were tested to determine the effect of polymeric matrix on the mechanical properties of CPP filler. The hardness test was carried out using Zwick 3150 Hardness Tester, Germany. The average value for each test was taken for ten readings to confirm the results. The compressive strength was measured for the prepared composites by using tensile testing machine, Zwick Z010, Germany. The average value for each test was taken for three samples to verify the results. The shape of sample was cylindrical (1 cm × 1 cm), load cell was 10 kN and crosshead speed was 10 mm/min.

2.5. Bioactivity behavior

Standard *in vitro* bioactivity test was carried out to evaluate the formation of an apatite layer onto the surface of the copolymer and composite samples. In order to study the bioactivity, the samples were soaked in simulated body fluid (SBF) which was proposed by Kokubo et al. [27] at 37 °C and

Table 1
The grafting % and weight loss of the prepared samples.

Sample	CPP powder	Copolymer	CPP/chitosan comp.	CPP/chitosan–gelatin comp.
G%	–	1465	2592	2066
Weight loss (%)	0.13	98.53	51.1	47.1
Attached copolymer (%)	–	–	50.96	46.97

pH 7.4 for several periods of times up to 28 days. The SBF has a composition similar to human blood plasma and has been extensively used for *in vitro* bioactivity test. After immersion, the specimens were removed from the SBF solution and were abundantly rinsed with deionized distilled water in order to remove the soluble inorganic salts and to stop the reaction. Total calcium and phosphorus ions were measured in SBF after withdrawal of the samples using spectrophotometer at $\lambda = 602\ cm^{-1}$ for calcium ions and at $\lambda = 575\ cm^{-1}$ for phosphorus ions using biochemical kits.

2.6. Statistical analysis

All samples analyzed in triplicate and the experiments were performed three times. Statistical analysis was performed using a *t*-test. The level of significance is set at $p < 0.05$.

3. Results and discussion

3.1. Preparation of CPP filler powder

The CPP compound is produced under the effect of thermal treatment of burshite powder at 800 °C with the release of structural water according to the following equations:

$$2CaHPO_4{\cdot}2H_2O \rightarrow 2CaHPO_4 + 4H_2O\uparrow$$

$$2CaHPO_4 \rightarrow Ca_2P_2O_7 + H_2O\uparrow$$

The TGA data proved that the destruction of burshite started at about 350 °C and ended at 470 °C with the weight loss (2.494%). The presence of endothermic peak at about 470 °C with the release of structural water proving the destruction of burshite compound to calcium hydrogen phosphate which is converted to CPP compound with the continuity of raising firing temperature accompanying the release of the remaining structural water.

3.2. The grafting (G%) and TGA analysis

The *G%* of the copolymer recorded 1465 which was lower than the grafting % of the copolymer in the presence of the filler (2592 and 2066%) as in CPP/chitosan and CPP/chitosan–gelatin composites, respectively, proving the presence of chitosan into the polymeric matrix at the expense of gelatin enhanced the grafting % of HEMA monomer onto chitosan polymer. This result confirms that the presence of CPP particles into the co-polymeric matrix increased the *G%* especially in the presence of the grafted chitosan polymer compared to those composites containing chitosan–gelatin matrix. This result is due to the diffusion of free radicals arising from CAN initiator which forms more hydrogen bonding between chitosan and HEMA leading to enhancement of the grafting of HEMA monomer onto chitosan polymer compared to that of chitosan–gelatin polymers. Table 1 shows the weight loss of the CPP powder and its composites with the co-polymeric matrix. The attached copolymer layer onto the surface of particles for CPP/chitosan and CPP/chitosan–gelatin composites recorded 50.955 and 46.965%, respectively; these data were calculated from the difference between the weight loss of the CPP powder and the composite. This result indicates that the affinity of CPP powder to chitosan co-polymeric matrix was more pronounced compared to chitosan–gelatin polymeric matrix, therefore, the TGA data was coincided with the grafting data.

3.3. Characterization of the composites

3.3.1. Phase analysis (XRD)

Fig. 1 shows XRD of chitosan powder and grafted chitosan copolymer. Fig. 1b shows that the patterns of chitosan into the copolymer structure have broad hump with lower intensity and some shift to lower angle compared to the original chitosan (Card No: 39-1894) proving chemical interaction between chitosan polymer and HEMA monomer. This result is coincided with the reported work which concluded that the wide peak assigning to chitosan was sharper and broader with some shift to lower angle after grafting process of chitosan [28]. For CPP filler powder and its composites with co-polymeric matrix, the characteristic peaks of CPP powder appear in the range of 2θ (25–35)° and the patterns of CPP powder have three main peaks at *d*-spacing (Å) equal 3.22, 3.09 and 3.02 (Card No: 20-0024) proving formation of CPP compound (Fig. 2a). These peaks are still persisted in both composites (CPP/chitosan and CPP/chitosan–gelatin composites) with lower peaks intensity compared to CPP powder proving coating, especially the CPP composite containing grafted chitosan in its structure. The chitosan or chitosan–gelatin peaks of co-polymeric matrix in both CPP composites disappeared due to effect of the CPP particles and amorphous nature of co-polymeric matrices (Fig. 2b and c).

3.3.2. FT-IR analysis

FT-IR spectrum of grafted chitosan copolymer sample is shown in Fig. 3a. The band appeared at 3435 cm^{-1} is assigned to OH^- group characterizing structure of chitosan and pHEMA structure. The bands at 523 and 899 cm^{-1}, 1454, and 1385 cm^{-1} are assigned to CH, CH_2 and CH_3, respectively. Also, two bands at 850 and 749 cm^{-1} are assigned to CH band [29]. Additionally, the bands at range of 1026–1159, 1273 and 1726 cm^{-1} are

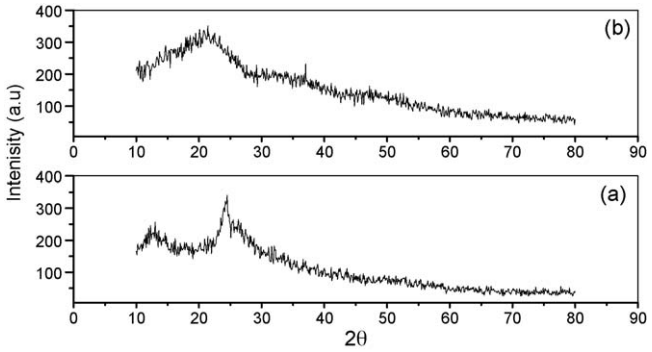

Fig. 1. XRD of (a) chitosan and (b) copolymer.

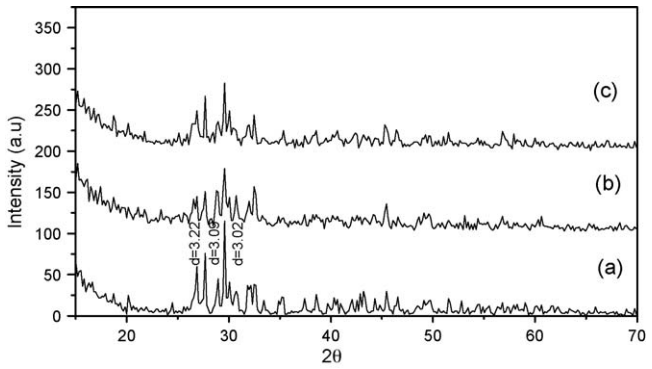

Fig. 2. The XRD of (a) CPP powder, (b) CPP/chitosan composite and (c) CPP/chitosan–gelatin composite.

assigned to C–O, CCO and C=O groups, respectively, characterizing the copolymer structure. The band at 1638 cm^{-1} is assigned to amide I which characterizes chitosan structure (Fig. 3a) [30]. FT-IR spectrum of CPP powder is shown in Fig. 3b. The sharp peaks at 1186–941 and 726 cm^{-1} are attributed to phosphate stretching and bending mode of vibration, respectively. Other bands at 613–494 cm^{-1} are due to phosphate bending mode of vibrations. Finally, the bands at 3432 and 1644 cm^{-1} are corresponding to OH and/or absorbed water [31].

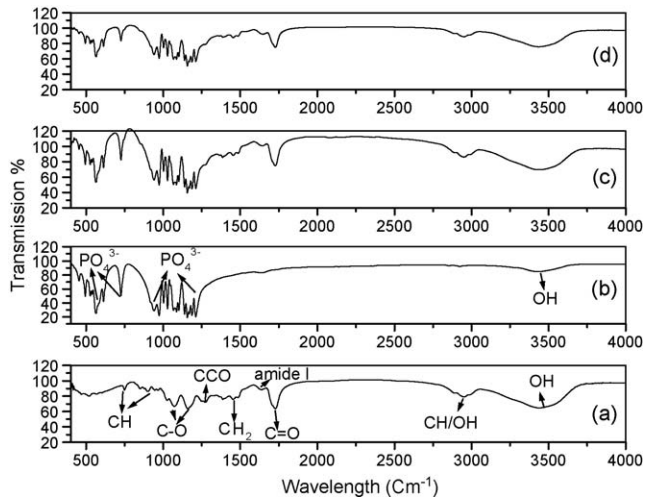

Fig. 3. FT-IR of (a) grafted chitosan copolymer, (b) CPP powder, (c) CPP/chitosan composite and (d) CPP/chitosan–gelatin composite.

After the loading process, for CPP/chitosan composite, all the characteristic bands for CPP powder are still appeared in the spectrum of CPP/chitosan composite such as the sharp peaks of the asymmetrical terminal P–O stretching mode at 1186, 1170, 1157, 1138, 1102, 1086 and 1066 cm^{-1}, the sharp peaks of the symmetric terminal P–O stretching vibration at 1028 and 1002 cm^{-1}, the bands of the bridge P–O asymmetric stretching mode at 972 and 941 cm^{-1}, the sharp peak of the bridge P–O symmetric stretching mode at 726 cm^{-1}, the bands of the terminal P–O asymmetrical bending mode at 613, 565, 539 and 527 cm^{-1} and the band of the terminal P–O symmetrical stretching mode at 494 cm^{-1} found in the spectrum of composite but they have lower optical density (O.D.) compared to the original CPP powder denoting coating effect (Fig. 3c). The reduced O.D. indicates that CPP particles are coated with the polymeric layer. In addition, the characteristic bands for copolymer structure, such as CH, CH_2 and CH_3, C–O, CCO, C=O and amide are still appeared in the spectrum composite. Also, they had lower O.D. compared to the original grafted chitosan copolymer proving effect of CPP particles on these sites of bands. Therefore, the formation of CPP/chitosan composite was conformed.

For CPP/chitosan–gelatin composite, the bands of CPP are still appeared in the spectrum of the composite, but they have a lower O.D. compared to the original CPP sample and CPP/chitosan composite sample (Fig. 3d). The reduced O.D. peaks indicate that CPP particles are also coated with the chitosan–gelatin polymeric layer. On the other hand, the characteristic bands for chitosan copolymer structure such as CH, CH_2 and CH_3, C–O, CCO, C=O and amide are still appeared and had very lower O.D. compared to the original grafted chitosan copolymer and CPP/chitosan composite proving effect of filler on the polymer sites. In addition, FT-IR proves that the coating process onto the CPP particles was achieved for both CPP/polymeric composites.

3.4. Mechanical testing

Table 2 shows the hardness and compressive strength of copolymer (chitosan-grafted copolymer) and its composites with CPP filler powder. It was notified that hardness of CPP/chitosan composite (66.80) was increased compared to chitosan copolymer (60.88) and the hardness of CPP/chitosan-grafted composite (68.23) was also increased compared to chitosan–gelatin copolymer (84.12). The reason of this behavior is due to the presence of small particle size of CPP powder into the copolymer matrix proving the polymer/filler interaction and adhesion. Also, the compressive strength of CPP/chitosan composite (6.53 MPa) was increased compared to chitosan copolymer (5.11 MPa) and the compressive strength of CPP/chitosan-grafted composite (6.26 MPa) was slightly increased compared to chitosan–gelatin copolymer (6.14 MPa). This result proves that the loading of fixed weight from CPP filler powder onto chitosan copolymer or chitosan–gelatin copolymer leads to the enhancement of the mechanical properties of the CPP/polymeric composite. The values of compressive strength are comparable to those of human cancellous bone

Table 2
Mechanical properties of the copolymer and its composites with CPP compared to human cancellous bone.

Test	Sample				
	Chitosan copolymer	CPP/chitosan composite	Chitosan–gelatin copolymer	CPP/chitosan–gelatin composite	Cancellous bone
Compressive strength (MPa)	5.1 ± 0.2	6.5 ± 0.1	6.1 ± 0.2	6.3 ± 0.2	2–12
Hardness (MPa)	60.9 ± 0.8	66.8 ± 0.9	68.2 ± 0.8	84.1 ± 1.1	–

[32]. As a result, CPP filler powder into the copolymer matrix containing chitosan or chitosan–gelatin polymer resulted in more effective reinforcement of the composite, then, stiffer composite.

3.5. Water absorption (W.A %)

Fig. 4 shows water absorption of the copolymer and its composite with CPP powder. The data show that the W.A % for all samples were high at initial time (after 24 h), then these values were gradually reduced to reach minimum values (after 7 days). The grafted chitosan copolymer had high W.A % values compared to other samples proving high affinity of the copolymer to water molecules because it contains a lot of OH groups in its structure.

While the CPP/chitosan–gelatin composite had minimum values for W.A % proving low affinity of this composite to water molecules due to the reduction in content of OH as a result of the diminishing content of chitosan at the expense of gelatin polymer. This result confirmed that the CPP/chitosan–gelatin composite had enhanced stability in distilled water compared to CPP/chitosan composite due to it has low content of OH molecules in its structure.

3.6. Bioactivity test

3.6.1. Total calcium ions

Fig. 5 shows the mean value of calcium ions concentration in SBF for copolymer, CPP and their composites post-immersion as compared to control. Calcium ion concentration for all samples post-immersion in SBF was significantly lower than control at all periods indicating the deposition of calcium ions on the surface especially for copolymer [33] and CPP samples and after longer time Calcium ions concentration for CPP/chitosan composite in SBF was reduced compared with control and CPP/chitosan–gelatin composite at all periods proving the deposition of calcium ions on the composite surface containing chitosan structure. This result confirms that the presence of chitosan into CPP/composite accelerates the deposition of calcium ions while the presence of gelatin leads to decrease of its deposition confirming biodegradation feature of gelatin. Calcium ion concentration for CPP/chitosan–gelatin composite

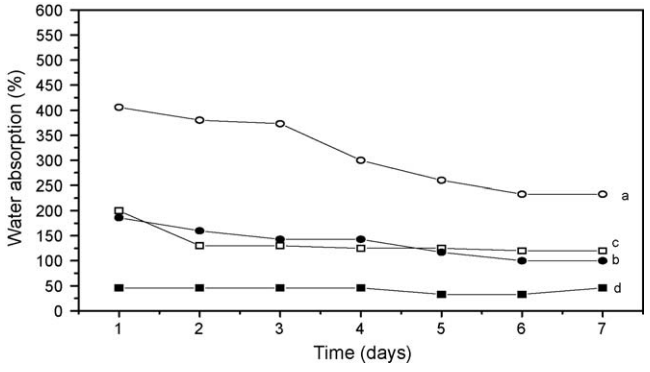

Fig. 4. Water absorption % of (a) grafted chitosan copolymer, (b) CPP/chitosan composite, (c) chitosan–gelatin copolymer and (d) CPP/chitosan–gelatin composite.

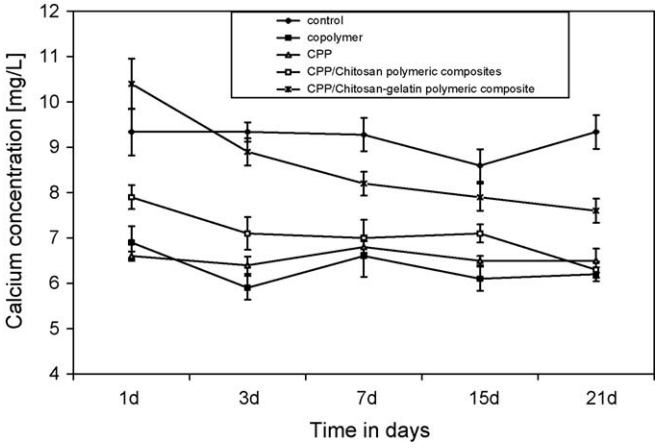

Fig. 5. Mean of calcium ions concentration in SBF post-immersion of the prepared samples compared to control (±S.D.; $n = 3$). Statistical analysis was performed using Student's t-test and the level of significance was set at $p < 0.05$.

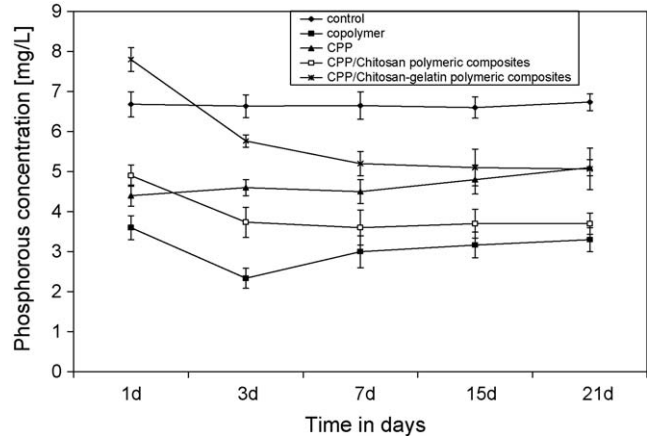

Fig. 6. Mean of phosphate ions concentration in SBF post-immersion of the prepared samples compared to control (±S.D.; $n = 3$). Statistical analysis was performed using Student's t-test and the level of significance was set at $p < 0.05$.

was higher than control post-immersion for 1 day. Statistical analyses show that the increase was significant proving degradation of composite with release of calcium ion, this result is due to the addition of gelatin to the composite. Then it started to be significantly decreased after 3 days of immersion compared to control at all other periods indicating deposition of calcium ions on the composite surface. At the same time, these values of calcium ions were increased for CPP/chitosan–gelatin composite compared to copolymer and CPP/chitosan composite at all periods confirming the presence of gelatin into the CPP composite resulted in the enhancement of its degradation causing more calcium ion to be released from its surfaces proving the vital role of gelatin in the biodegradation process and improvement of bioactivity.

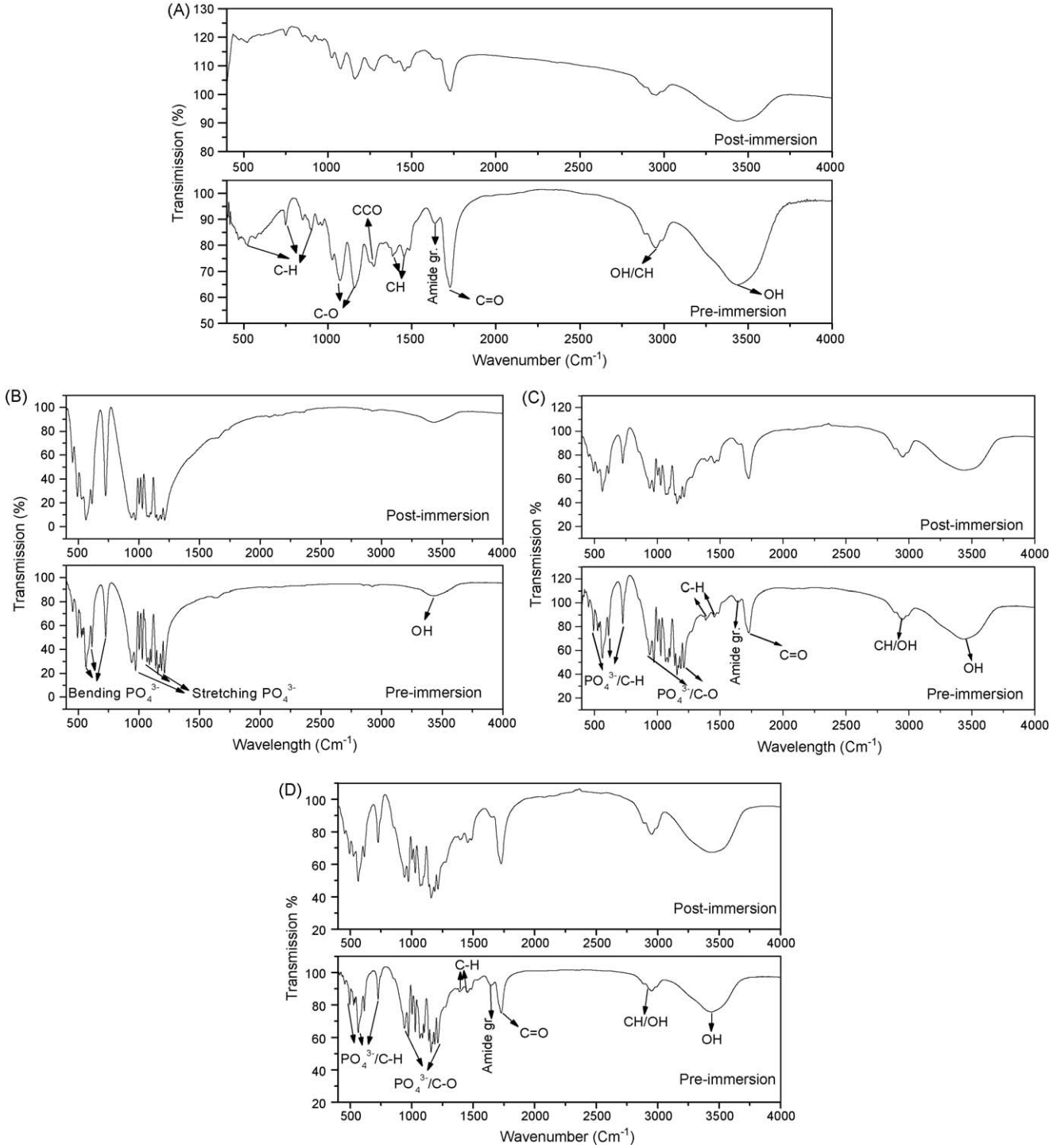

Fig. 7. (A) The FT-IR of grafted chitosan copolymer sample pre- and post-immersion in SBF for 21 days. (B) The FT-IR of CPP sample pre- and post-immersion in SBF for 21 days. (C) FT-IR of CPP/chitosan composite pre- and post-immersion in SBF for 21 days. (D) FT-IR of CPP/chitosan–gelatin composite pre- and post-immersion in SBF for 21 days.

3.6.2. Phosphorus ions

Fig. 6 shows the mean value of phosphorus ions concentration in SBF post-immersion of copolymer, CPP, CPP/chitosan and CPP/chitosan–gelatin composites compared to control. Phosphorus ion concentration in SBF post-immersion of all samples was significantly reduced compared to control (SBF) at all periods indicating the deposition of phosphorus ions on the material surface of the samples especially copolymer sample. Phosphorus ions concentration in SBF post-immersion of CPP/chitosan composite was significantly reduced compared with control, CPP

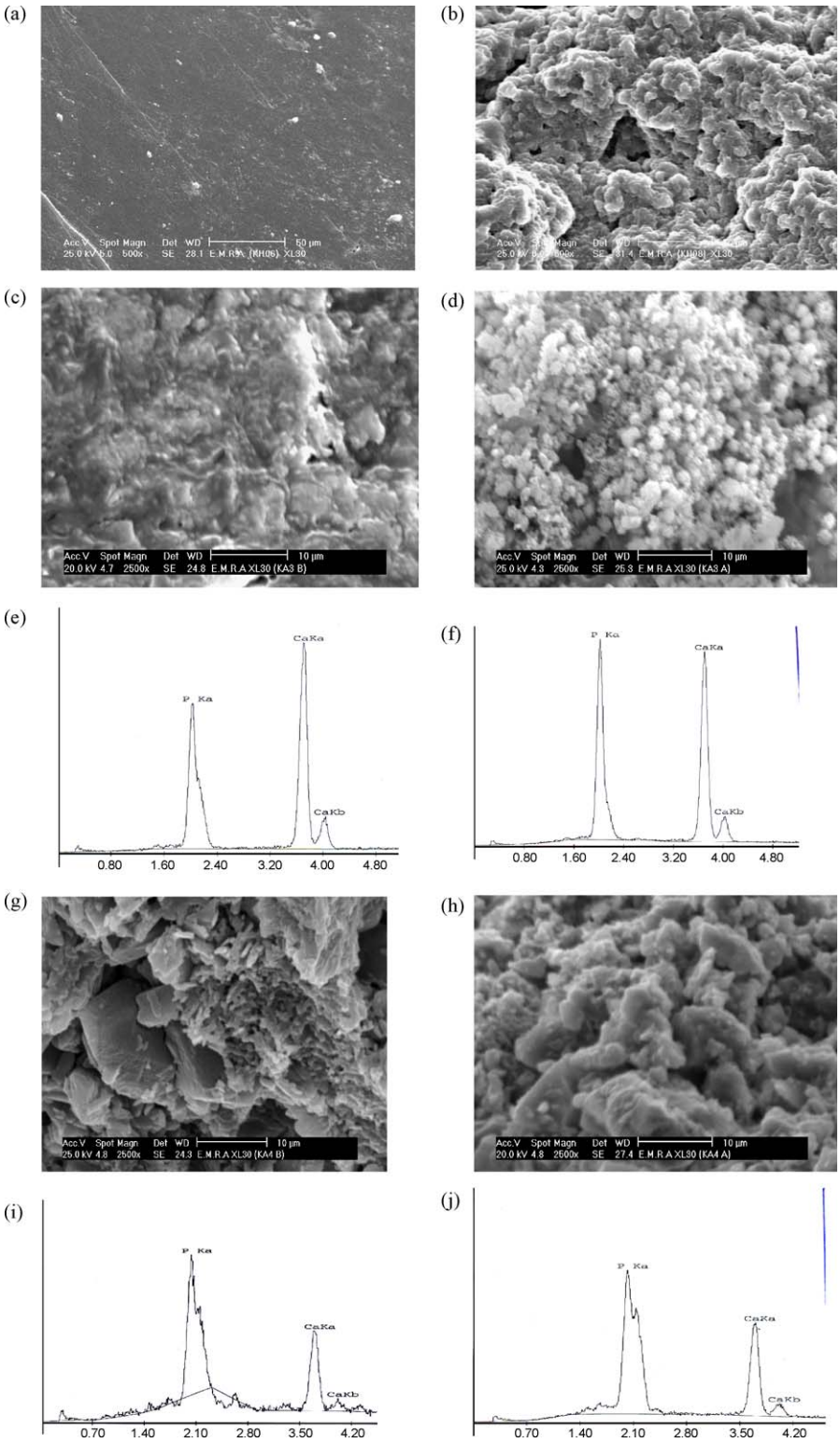

Fig. 8. SEM of copolymer (a) pre- and (b) post-immersion, CPP/chitosan composite (c) pre- and (d) post-immersion, its EDAX analysis of (e) pre-and (f) post-immersion, SEM CPP/chitosan–gelatin composite (g) pre- and (h) post-immersion and its EDAX analysis of (i) pre- and (j) post-immersion.

and CPP/chitosan–gelatin composite at all time periods proving the deposition of phosphorus ions on the composite surface. This result confirms that the presence of chitosan into CPP/composite accelerates the deposition of phosphorus ions while the presence of gelatin leads to the slow of its deposition confirming biodegradation feature of gelatin. Phosphorus ion concentration in SBF post-immersion of CPP/chitosan–gelatin composite for 1 day was higher than control. Statistical analysis showed that this increase was significant proving degradation of composite with release of phosphorus ions; this result is due to the addition of gelatin to the CCP/chitosan composite. Then it started to be significantly decreased after 3 days of immersion compared to control and at all the other time periods indicating deposition of phosphorus ions on the composite surface. At the same time, these values of phosphorus ions were significantly increased for CPP/chitosan–gelatin composite compared to copolymer and CPP/chitosan composite at all time periods confirming that the presence of gelatin into the CCP/chitosan composite resulted in the enhancement of its degradation causing more phosphorus ion to be released from its surfaces proving the vital role of gelatin in the biodegradation process and in improvement of bioactivity. From the results of calcium and phosphorus ions, the CPP/chitosan composite had enhanced ability to accelerate calcium and phosphorus ions onto the composite surface compared to CPP/chitosan–gelatin composite surface, then, it can able to induce apatite layer formation onto the surface.

3.7. Characterization of composites pre- and post-immersion

3.7.1. FT-IR analysis

For copolymer, the O.D. of the polymer bands such as OH, C–H, amide group, C–O, C=O and CCO groups are reduced post-immersion compared to pre-immersion proving effect of immersion and their involvement in the biolayer formation or its masking due to the effect of mineralization on these sites (Fig. 7A). For CPP sample, the O.D. of phosphate groups (stretching vibration: 1200, 1170, 1070, 1020, 980 and 930 cm^{-1}) and (bending: 725, 605, 560 and 490 cm^{-1}) were more pronounced for post-immersion compared to pre-immersion proving deposition of phosphate ions on the surface from SBF. This result shows that the CPP sample may have ability to induce the apatite layer on its surface (Fig. 7B). For CPP/chitosan and CPP/chitosan–gelatin composites, Fig. 7C and D, show that the O.D. of phosphate bands and OH groups overlapping with polymer bands were enhanced post-immersion compared to pre-immersion proving deposition of some ions on the surface as a result of interaction between chitosan via amino groups and phosphate ions from SBF [33]. In addition, the O.D. of these bands was slightly increased for CPP/chitosan–gelatin composite compared to CPP/chitosan composite post-immersion (Fig. 7C and D) denoting the presence of gelatin polymer hydrolyzes to form carboxyl groups resulting in apatite nucleation [34].

3.7.2. Surface morphology

Fig. 8a shows SEM of chitosan–gelatin copolymer pre-immersion in SBF for 21 days. It indicates the presence of smooth surface proving homogeneity and interaction between both polymers and HEMA monomer confirming chemical interaction. While post-immersion, Fig. 8b appears the accumulation of spherical particles with bright color containing minute pores denoting formation and nucleation of apatite layer. For CPP/chitosan composite, at the same magnification (2500×), pre-immersion, Fig. 8c shows the presence of smooth and rough surfaces with some bright color and irregular shapes proving compatibility and cross linking between CPP filler and polymeric matrix. Post-immersion, Fig. 8d shows the appearance of many and concentrated spherical particles onto the surface of composite material denoting the formation and nucleation of apatite layer. EDAX analysis (Fig. 8e and f) shows that the value of Ca/P ratio is increased from (0.8) pre-immersion to (1.3) post-immersion confirming growth of apatite layer on the surface and coinciding with SEM results. For CPP/chitosan–gelatin composite, at the same magnification (2500×), pre-immersion, Fig. 8g indicates very characteristic structure of the composite containing minute and irregular large pores spreading onto the surface proving homogeneity and integration. Post-immersion, Fig. 8h shows the presence of many large irregular crystals proving nucleation of apatite layer with some bright color and some large pores distributed on the surface which is an important for bone ingrowth indicating effect of immersion and corrosion. Also, EDAX analysis (Fig. 8i and j) confirmed the increase of Ca/P ratio from (1.11) pre-immersion to (1.5) post-immersion proving enhancement of apatite nucleation coinciding with SEM results. The SEM-EDAX and FT-IR data post-immersion confirmed the formation of apatite layer onto the surface of the prepared biocomposites especially CPP/chitosan gelatin composite denoting the presence of gelatin in this composite enhanced apatite formation due to gelatin has high bioactivity properties.

4. Conclusion

The grafting, TGA, XRD, and FTIR results confirmed that the prepared composites containing CPP powder into the copolymer matrix containing the grafted chitosan or grafted chitosan–gelatin had enhanced coating from the copolymer matrix onto surface particles. Compressive strength of the CPP/polymeric composites had values comparable to those of cancellous bone. Water absorption property of CPP/chitosan–gelatin composite had high stability compared to CPP/chitosan composite proving low content of OH molecules in its structure resulting the stability of the produced composite. *In vitro* test results via calcium and phosphate ions measurements confirmed that the CPP/chitosan composite had slightly enhanced ability to accelerate the mineralization of calcium phosphate layer on its surface compared to CPP/chitosan–gelatin composite surface proving the vital role of chitosan polymer in the mineralization process. FT-IR and SEM provided by EDAX post-immersion confirmed that CPP/chitosan and/chitosan–gelatin polymeric composites lead to the formation of apatite onto their surfaces especially these CPP composites containing chitosan–gelatin matrices. Finally, novel CPP/chitosan or chitosan–gelatin biocomposites have bioactivity properties could be used in bone substitutes and tissue engineering applications.

References

[1] H.H. de Boer, The history of bone grafts, Clin. Orthop. Relat. Res. 226 (1988) 292–298.

[2] M.M. Pereira, J.R. Jones, L.L. Hench, Bioactive glass and hybrid scaffolds prepared by sol–gel method for bone tissue engineering, Adv. Appl. Ceram. 104 (1) (2005) 35.

[3] M. Wang, Developing bioactive composite materials for tissue replacement, Biomaterials 24 (2003) 2133–2151.

[4] S. Teng, J. Shi, B. Peng, L. Chen, The effect of alginate addition on the structure and morphology of hydroxyapatite/gelatin nanocomposites, Compos. Sci. Technol. 66 (2006) 1532–1538.

[5] V.V. Meretoja, A.O. Helminen, J.J. Korventausta, V. Haapa-aho, J.V. Seppälä, T.O. Närhi, Crosslinked poly(ε-caprolactone/D,L-lactide)/bioactive glass composite scaffolds for bone tissue engineering, J. Biomed. Mater. Res. 77A (2006) 261–268.

[6] P. Van Landuyt, F. Li, J.P. Keustermans, J.M. Streydio, F. Delannay, E. Munting, The influence of high sintering temperatures on the mechanical properties of hydroxyapatite, J. Mater. Sci. Mater. Med. 6 (1995) 8–13.

[7] Y.M. Khan, D.S. Katti, C.T. Laurencin, Novel polymer-synthesized ceramic composite-based system for bone repair: an *in vitro* evaluation, J. Biomed. Mater. Res. A 69 (2004) 728–737.

[8] G. Wei, P.X. Ma, Structure and properties of nano-hydroxyapatite/polymer composite scaffolds for bone tissue engineering, Biomaterials 25 (19) (2004) 4749–4757.

[9] C.M. Agrawal, R.B. Ray, Biodegradable polymeric scaffolds for musculoskeletal tissue engineering, J. Biomed. Mater. Res. 55 (2001) 141–150.

[10] K. Rezwan, Q.Z. Chen, J.J. Blaker, A.R. Boccaccini, Biodegradable and bioactive porous polymer/inorganic composite scaffolds for bone tissue engineering, Biomaterials 27 (18) (2006) 3413–3431.

[11] J. Berger, M. Reist, J.M. Mayer, O. Felt, N.A. Peppas, R. Gurny, Structure and interactions in covalently and ionically crosslinked chitosan hydrogels for biomedical applications, Eur. J. Pharm. Biopharm. 57 (2004) 19–34.

[12] S. Miyazaki, K. Ishii, T. Nadai, The use of chitin and chitosan as drug carriers, Chem. Pharm. Bull. 29 (1981) 3067.

[13] S.V. Madihally, H.W.T. Matthew, Porous chitosan scaffolds for tissue engineering, Biomaterials 20 (1999) 1133–1142.

[14] Y. Zhang, M.Q. Zhang, Three-dimensional macroporous calcium phosphate bioceramics with nested chitosan sponges for load-bearing bone implants, J. Biomed. Mater. Res. 61 (1) (2002).

[15] W.I. Abd El-Fattah, M. Samir, K.R. Mohamed, Modified HA/pHEMA-g-chitosan copolymer composites, in: Int. Conf. of Polymer Science, Sharm El-Shikh, Egypt (9/2001), 2001.

[16] L. Kong, Y. Gao, G. Lu, Y. Gong, N. Zhao, X. Zhang, A study on the bioactivity of chitosan/nano-hydroxyapatite composite scaffolds for bone tissue engineering, Eur. Polym. J. 42 (2006) 3171–3179.

[17] H.W. Kim, H.E. Kim, V. Salih, Stimulation of osteoblast responses to biomimetic nanocomposites of gelatin–hydroxyapatite for tissue engineering scaffolds, Biomaterials 26 (2005) 5221–5230.

[18] W.Y. Xia, W. Liu, L. Cui, Y.C. Liu, W. Zhong, D.L. Liu, et al., Tissue engineering of cartilage with the use of chitosan–gelatin complex scaffolds, J. Biomed. Mater. Res. 71B (2004) 373–380.

[19] F. Zhao, W.L. Grayson, T. Ma, B. Bunnell, W.W. Lu, Effects of hydroxyapatite in 3-D chitosan–gelatin polymer network on human mesenchymal stem cell construct development, Biomaterials 27 (2006) 1859–1867.

[20] J. Kunzler, J. McGee, Contact lens materials, Chem. Ind. 16 (1995) 651–655.

[21] C.P.A.T. Klein, A.A. Driessen, K. Degroot, A. Vandenhooff, Biodegradation behavior of various calcium–phosphate materials in bone tissue, J. Biomed. Mater. Res. 17 (5) (1983) 769–784.

[22] W.E. Brown, N. Eidelman, B. Tomazic, Octacalcium phosphate a precursor in biomineral formation, Adv. Dent. Res. 1 (1987) 306–313.

[23] S. Kamakura, Y. Sasano, H. Homma, O. Suzuki, H. Ohki, M. Kagayama, K. Motegi, Implantation of octacalcium phosphate (OCP) in rat skull defects enhances bone repair, J. Dent. Res. 78 (1999) 1682–1687.

[24] P. Ducheyne, Bioceramics: material characteristics versus *in vivo* behavior, J. Biomed. Mater. Res. 21 (A2 Suppl) (1987) 219–236.

[25] J.S. Sun, Y.H. Tsuang, C.J. Liao, H.C. Liu, Y.S. Hang, F.H. Lin, The effects of calcium phosphates particles on the growth of osteoblast, J. Biomed. Mater. Res. 37 (1997) 324–334.

[26] A. Lagos, J. Reyes, Grafting onto chitosan. I. Graft copolymerization of methylmethacrylate onto chitosan with Fenton's reagent (Fe^{2+}–H_2O) as a redox initiator, J. Polym. Sci. 26 (1988) 985–991.

[27] T. Kokubo, H.M. Kim, M. Kawashita, H. Takadama, T. Miyazaki, M. Uchida, T. Nakamure, Nucleation and growth of apatite on amorphous phases in simulated body fluid, Glastech. Ber. Glass Sci. Technol. 73 (2001) 247–254.

[28] K.V.H. Prashanth, R.N. Tharanathan, Q. Hu, B. Li, M. Wang, J. Shen, Preparation and characterization of biodegradable chitosan/hydroxyapatite nanocomposite rods via in situ hybridization: a potential material as internal fixation of bone fracture, Biomaterials 25 (2004) 779–785.

[29] K.R. Mohamed, G.T. El-Bassyouni, H.H. Beherei, Chitosan graft copolymers-HA/DBM biocomposites: preparation, characterization, and *in vitro* evaluation, J. Appl. Polym. Sci. 105 (2007) 2553–2563.

[30] A.L. Oliveira, P.B. Malafaya, R.L. Reis, Sodium silicate gel as precursor for the in vitro nucleation and growth of a bone-like apatite coating in compact and porous polymeric structures, Biomaterials 24 (2003) 2575–2584.

[31] F. Chen, Z. Wang, C. Lin, Preparation and characterization of nano-sized HA particles and HA/chitosan nano-composite for use in biomedical materials, Mater. Lett. 57 (2002) 858–861.

[32] T. Kokubo, H. Kim, M. Kawashita, Novel bioactive materials with different mechanical properties, Biomaterials 24 (2003) 2161–2175.

[33] V. Vinchent, C. Breandon, G. Nihoul, J.R. Gavarri, Eur. J. Solid State Inorg. Chem. 34 (1977) 571.

[34] Khaled R. Mohamed, Amani A. Mostafa, Preparation and bioactivity evaluation of hydroxyapatite-titania/chitosan–gelatin polymeric biocomposites, J. Mater. Sci. Eng. C 28 (2008) 1087–1099.